JMEPEG (2010) 19:721–727
DOI: 10.1007/s11665-009-9534-3

1059-9495/$19.00

Microstructure and Corrosion Behavior of CrN and CrSiCN Coatings

Feng Cai, Qi Yang, Xiao Huang, and Ronghua Wei

(Submitted April 20, 2009; in revised form July 6, 2009)

Three CrN-based coatings were deposited on 17-4PH stainless steel substrate using plasma enhanced magnetron sputtering (PEMS) technique. The microstructure and corrosion resistance were evaluated to examine the effect of Si and C in the coatings. The three coating compositions were CrN($Cr_{0.69}N_{0.31}$), CrSiCN-1 ($Cr_{0.55}Si_{0.014}C_{0.14}N_{0.3}$), and CrSiCN-2 ($Cr_{0.43}Si_{0.037}C_{0.24}N_{0.3}$). The testing results indicated that with the increase of Si concentration, the coating microstructure transformed from B1 structure to B1 + Si_3N_4 structure. All the three coating systems were subjected to electrochemical tests in 3.5% NaCl solution at room temperature. Potentiodynamic polarization results revealed that the CrSiCN-2 coating had a higher anodic current density and a lower corrosion potential when compared to the CrN and CrSiCN-1 coatings. Extended exposure in 3.5% NaCl caused several localized corrosion to the CrSiCN-2 coating due to the porous coating structure. Electrochemical impedance spectroscopic measurements demonstrated that the CrSiCN-1 has better corrosion resistance than CrN and CrSiCN-2.

Keywords corrosion, CrN, CrSiCN, microstructure, PVD coating

1. Introduction

Chromium-based nitride coatings are well known for their higher ductility and fracture toughness, lower coefficient of friction, and excellent oxidation and corrosion resistances comparing with the widely used TiN counterparts (Ref 1-3). A distinguish advantage of CrN coatings over TiN coatings is their excellent wear resistance under dry sliding conditions, benefiting from their lower friction coefficient. In the field of erosive applications, their higher toughness prevents crack initiation and propagation (Ref 4) thus reducing the erosion damage in CrN coatings. In particular, CrN coatings have been employed to protect cutting tools for machining Cu-, Al-, and Ti-based alloys (Ref 5), and became successful alternative coating system to TiN in protecting die casting tools (Ref 6). However, CrN coatings have very limited applications in other industries due to their low hardness. Alloying addition and microstructure modification to CrN have been used to improve coating hardness and tribological performance. Combining the advantages of wear resistance of carbonitride and corrosion resistant Cr-based coatings (Ref 7), chromium carbonitride (CrCN) compounds have shown increased hardness values up to HV 2200 (comparing with that of CrN with the hardness in a range of 1500-2000 HV; Ref 8, 9), and improved wear performance over CrN and TiN coatings (Ref 3). Furthermore, it was reported that in addition to the hardness increase, corrosion and oxidation resistance of CrN coatings can be enhanced by the incorporation of Si within a certain concentration range (Ref 10, 11). Also, significant reduction in coefficient of friction can be realized by the incorporation of Si into CrN coatings (Ref 12-14). These modifications have brought impacts on mechanical properties of Cr-N based coatings; however, the information about the influence of Si addition on corrosion performances of CrSiCN coating systems is limited. As such this research intends to achieve further understanding of this series of coatings.

The objectives of this study are to characterize the coating microstructure changes as a result of the incorporation of Si and C in CrN coatings and the subsequent change in their corrosion behavior. The corrosion characteristics of these coatings were investigated through electrochemical tests, namely potentiodynamic polarization and electrochemical impedance spectroscopy (EIS) tests.

2. Experimental

17-4PH steel substrates were machined into disks and were polished to a mirror finish with 0.5 μm diamond paste. The deposition process was carried out using a plasma enhanced magnetron sputtering (PEMS) coater at Southwest Research Institute. Prior to coating deposition, substrates were sputtered with Ar for 60-90 min in order to remove any residual contaminant from the surface. A solid target of Cr was employed as a source of Cr (Ref 15) and a mixture of argon (Ar) and nitrogen (N_2) gases was introduced during the deposition process. To introduce Si into the coating composition, trimethylsilane ($(CH_3)_3SiH$ or TMS) was used as the precursor to form the series of $CrSi_xC_yN_z$ coatings. The chamber pressure was maintained in a range of 0.33 and

Feng Cai and **Xiao Huang**, Department of Mechanical and Aerospace Engineering, Carleton University, Ottawa, ON, Canada; **Qi Yang**, Institute for Aerospace Research, National Research Council, Ottawa, ON, Canada; and **Ronghua Wei**, Southwest Research Institute, San Antonio, TX. Contact e-mail: Qi.Yang@nrc-cnrc.gc.ca.

0.47 Pa (2.5-3.5 × 10^{-3} Torr) at the deposition stage. The surface temperature of the substrate was maintained at about 400 °C during the coating deposition process.

The coating surface morphologies were examined using scanning electron microscopy (SEM), and the chemical composition of the coatings was measured using energy dispersive x-ray spectroscopy (EDS). The crystal structure of the synthesized coating was determined using Rigaku x-ray diffractometer (XRD) with a CuK_α radiation source (λ = 0.1542 nm). The x-ray scan was taken in the 2θ range of 20° to 100° at a scan rate of 2.4°/min.

The corrosion performances of the coating systems were investigated using potentiodynamic polarization and EIS techniques. The test rig was a traditional three-electrode cell wherein a saturated calomel electrode (SCE) works as a reference electrode, and a graphite bar as a counter electrode. All the electrochemical tests were performed with a circular exposure surface of a diameter of 1.0 cm (0.785 cm^2 in area) in a 3.5-wt.% NaCl aqueous solution at room temperature. Process control and data acquisition were implemented using a Gamry potentiostat/galvanostat/ZRA system. Potentiodynamic polarization curves were obtained at a scan rate of 1 mV/s, starting from an initial potential of −300 mV versus the open circuit potential of the coated system to the final potential up to 1000 mV, and the change in the corrosion current density was measured. EIS was employed to reveal changes in the corrosion performance after extended exposure time. EIS spectra were performed with an alternate current (AC) signal of 10 mV peak to peak in amplitude superimposed on to the open circuit potential. The frequency range of the AC signal was from 300 kHz to 10 mHz. The EIS measurements started initially at 5 min, and then were carried out after several hours, and could be up to several days until a clear trend could be established. The test results were interpreted through curve fitting with an equivalent electrical circuit using Gamry Echem Analyst program.

3. Results and Discussion

3.1 Surface Morphologies of the Coatings

The surface morphologies of all three coatings are shown in Fig. 1, in which CrN and CrSiCN-1 exhibit (Fig. 1a, b) fine dense structure while CrSiCN-2 reveals a typical porous columnar structure (Fig. 1c). SEM analysis also revealed coating defects on the coating surfaces as illustrated in Fig. 2(a-c). This nodular type of defects often occurs during PVD process shown as embedded nodule originated from foreign particles or large droplets deposited on the coating surface. The presence of these nodular defects can weaken the bonding between successive coating layers and create gaps between the nodules and bulk coating, which can affect corrosion resistance of the coatings (Ref 16, 17).

3.2 Chemical Compositions and Crystallographic Structure of the Coatings

The chemical compositions of the three coatings were analyzed using EDS technique and the results are summarized in Table 1. The atomic percentages of Cr in each of the three coatings decreased when Si and C contents increased. The N content was consistent for all three coating compositions. Also shown in the table are the gas flow rates used to generate three compositions. It is to be noted that the Si content in CrSiCN-2 was selected to be above the solid solution limit of Si in Cr-Si-N system (7.3% atomic ratio of Si: (Si + Cr) in order to form Si_3N_4; Ref 18).

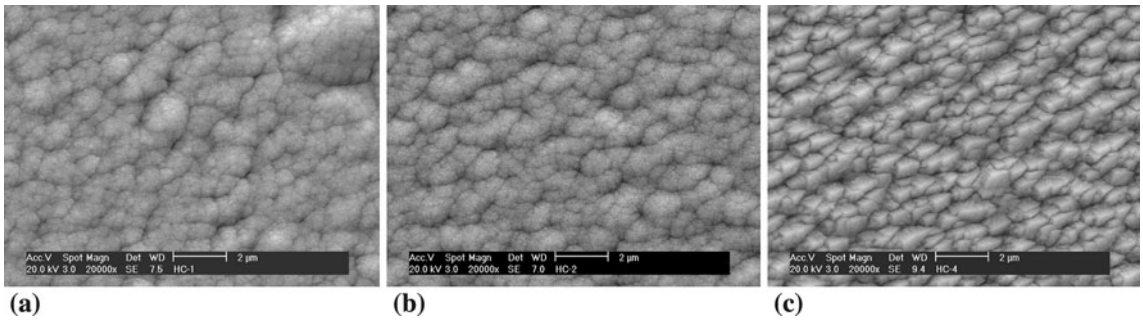

Fig. 1 Surface morphology of three-coating systems: (a) CrN, (b) CrSiCN-1, and (c) CrSiCN-2

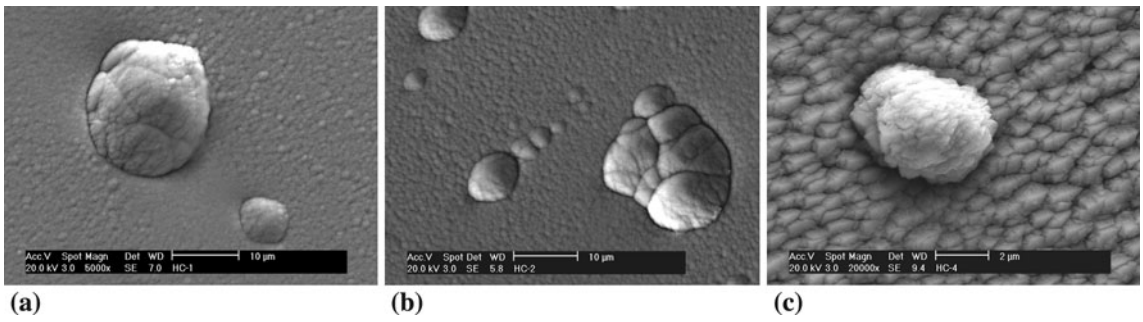

Fig. 2 Coating defects observed in (a) CrN, (b) CrSiCN-1, and (c) CrSiCN-2

Table 1 Coating process variables and chemical compositions (at.%)

Coating	N_2, sccm	TMS, sccm	Cr	Si	C	N
CrN	100	0	68.9	...	...	31.1
CrSiCN-1	100	3	55.3	1.4	13.9	29.5
CrSiCN-2	100	9	42.8	3.7 (7.9% for Si:(Cr + Si))	23.8	29.6

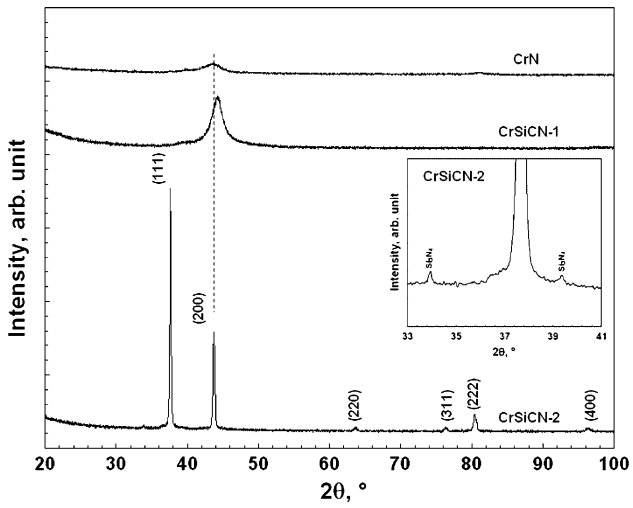

Fig. 3 X-ray diffraction spectra of CrN, CrSiCN-1, and CrSiCN-2

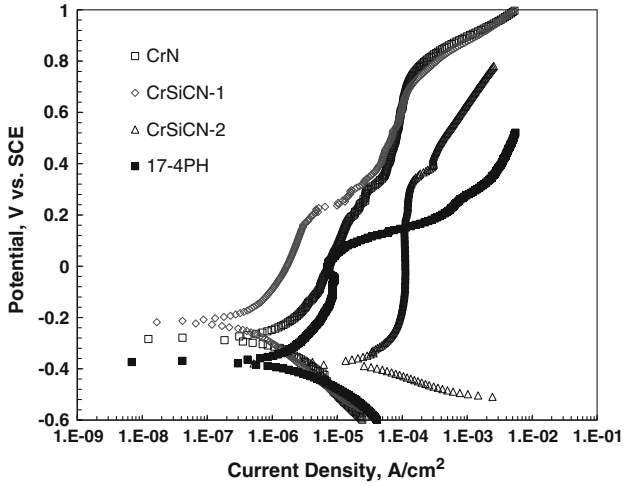

Fig. 4 Potentiodynamic polarization curves of three coatings and the substrate

Table 2 Summary of potentiodynamic polarization test results

Coating system	E_{corr}, mV	I_{corr}, μA/cm²	R_p, kΩ cm²	P
17-4PH	−374	1.70	18.9	...
CrN	−284	0.55	64.1	0.0025
CrSiCN-1	−218	0.37	176	0.00068
CrSiCN-2	−379	12.0	1.16	0.0569

The XRD spectra for the three coatings are shown in Fig. 3. The CrN coating have a face centered cubic B1 structure with a (200) preferred orientation. The CrSiCN-1 coating with a lower Si and C contents also has a phase with B-1 structure and stronger (200) preferred orientation. The CrSiCN-2 coating, with higher contents of Si and C, shows all the distinct diffraction peaks of B1 structure indicating no preferred orientations, as shown in Fig. 3. Comparing the diffraction pattern of CrSiCN-2 to those of CrSiCN-1 and CrN, the increased crystallinity of CrSiCN-2 is clearly observed. Furthermore, when slow-scanning the region around (111) B1 peak for sample CrSiCN-2, diffraction peaks from crystalline Si_3N_4 were found as illustrated by the inset in Fig. 3. This finding contradicts the published research where the addition of Si to CrN coating has been observed to induce the formation of amorphous Si_3N_4 around the boundary of the crystalline structure (Ref 10, 11, 15, 19-23). The reason(s) for the formation of crystalline Si_3N_4 is not certain at present.

Using Scherrer equation (Ref 24), the average grain size for each sample was calculated. The grain size decreased from 7.6 nm for CrN coating to 5 nm for CrSiCN-1 initially. From CrSiCN-1 to CrSiCN-2 (44.1 nm), an opposite trend of increased grain size was observed; this is consistent with the surface morphology observation where CrSiCN-2 exhibited a coarse columnar structure (Fig. 1c).

3.3 Potentiodynamic Polarization Measurements

Potentiodynamic polarization measurement is a traditional DC approach that can provide kinetic information of corrosion performance of a system (Ref 25). In this study, the polarization characteristics were measured for all the three coatings, and the corresponding curves are presented in Fig. 4.

All the three coatings demonstrated wide passive ranges comparing to the 17-4PH steel substrate (Fig. 4). In addition, both CrN and CrSiCN-1 coatings showed noticeable higher corrosion potentials and lower passive current densities than 17-4PH steel substrate. However, the coating CrSiCN-2 exhibited a similar corrosion potential to that of the bare substrate and the highest passive current density among all the samples.

Based on the polarization curves (Fig. 4), other corrosion characteristics such as the polarization resistance (R_p) and coating porosity (P) can be estimated using the following Eqs 1 and 2, respectively.

$$R_p = \frac{\beta_a \beta_c}{2.3039(\beta_a + \beta_c) I_{corr}} \quad \text{(Eq 1)}$$

where β_a and β_c are the Tafel slopes of anodic and cathodic regions. I_{corr} is the corrosion current density, and can be obtained through Tafel extrapolation from the curves (Ref 26, 27).

$$P = (R_{ps}/R_p) \times 10^{-|\Delta E_{corr}|/\beta_a} \quad \text{(Eq 2)}$$

where R_{ps} is the polarization resistance of the steel substrate, and ΔE_{corr} the difference in corrosion potentials between the coating and its steel substrate. The calculated R_p and P values are presented in Table 2.

The polarization resistance (R_p), which takes into consideration of both the corrosion current density and the slopes of polarization curves, can provide an overall ranking of coating's resistance to corrosion. As shown in Table 2, the coating

CrSiCN-1 possesses the highest polarization resistance, while CrSiCN-2 showed the lowest polarization resistance which is even lower than 17-4 PH substrate.

One of the primary concerns with PVD thin film coatings is the formation of pores and pinholes in the coating. The presences of these coating defects can unduly influence the corrosion performance of the coating layer and substrate by providing the accessing path of ions or solutions to the substrate surface. As such, in electrochemical analysis, porosity was measured as a means to compare the coating's integrity against corrosion. Form the results shown in Table 2 coating CrSiCN-1 demonstrated a significantly lower porosity than the other two coatings, in addition to higher polarization resistance. Similarly, CrSiCN-2 coatings revealed a high porosity, which leads to the lowest polarization resistance.

3.4 Electrochemical Impedance Spectroscopy Analysis

EIS was employed to nondestructively investigate the changes in the resistive-capacitive nature of electrochemical interfaces (Ref 28). It is particularly effective in studying the defects related degradation mode of coatings (Ref 29, 30). In this study, EIS data of the three coatings were taken after certain exposure times during the immersion in NaCl solution, in order to investigate the corrosion performance as a function of exposure time. A series of obtained data are presented in the forms of Nyquist plots and Bode plots as presented in Fig. 5 and 6, respectively.

The Nyquist plots (Fig. 5) for the coatings CrN, CrSiCN-1 and CrSiCN-2, are composed of a arc in the high frequency range and followed with an almost straight line. These straight lines indicate diffusion-controlled corrosion characteristics, especially in the low frequency ranges for all the coating specimens. The impedance values at low frequency for the coatings CrN and CrSiCN-1 reach the level of 100 kΩ cm^2 (Fig. 6), indicating excellent resistances to corrosion. Additionally, no significant change of the curves with immersion time indicates the stability in the corrosion performance of CrN and CrSiCN-1 (Fig. 5a, b). Whereas, the porous and dual-phase structured CrSiCN-2 demonstrates very low impedance values of 0.5 kΩ cm^2 (Fig. 6), showing a relatively poor corrosion resistance. These results demonstrate a consistence with those from potentiodynamic polarization measurements.

3.5 SEM Examination and Analyses After EIS Tests

After EIS tests, visual inspections did not find any rust and corrosion products on the tested CrN and CrSiCN-1 coatings after 7 days of immersion. SEM analysis also indicated that their surface morphology remained the same as the as-coated samples and EDS analyses further confirmed the lack of corrosion product. However, for the coating CrSiCN-2, visual inspection revealed discoloration after 1 h of immersion and the extent of surface corrosion intensified with increased exposure to the NaCl solution. SEM analysis of sample after 24 h exposure (Fig. 7a, b) demonstrated that the corrosive media had penetrated through the permeable pores (related coating defects such as those nodules observed in Fig. 2), and severe localized corrosion took place. The corrosion product surrounding the pit was observed and confirmed with SEM/EDS analyses, being rich in oxygen (O) and iron (Fe) (Fig. 7c). This clearly demonstrated that the corrosion medium has penetrated through the permeable pores and established galvanic corrosion cells between the exposed substrate surface and the coating. The

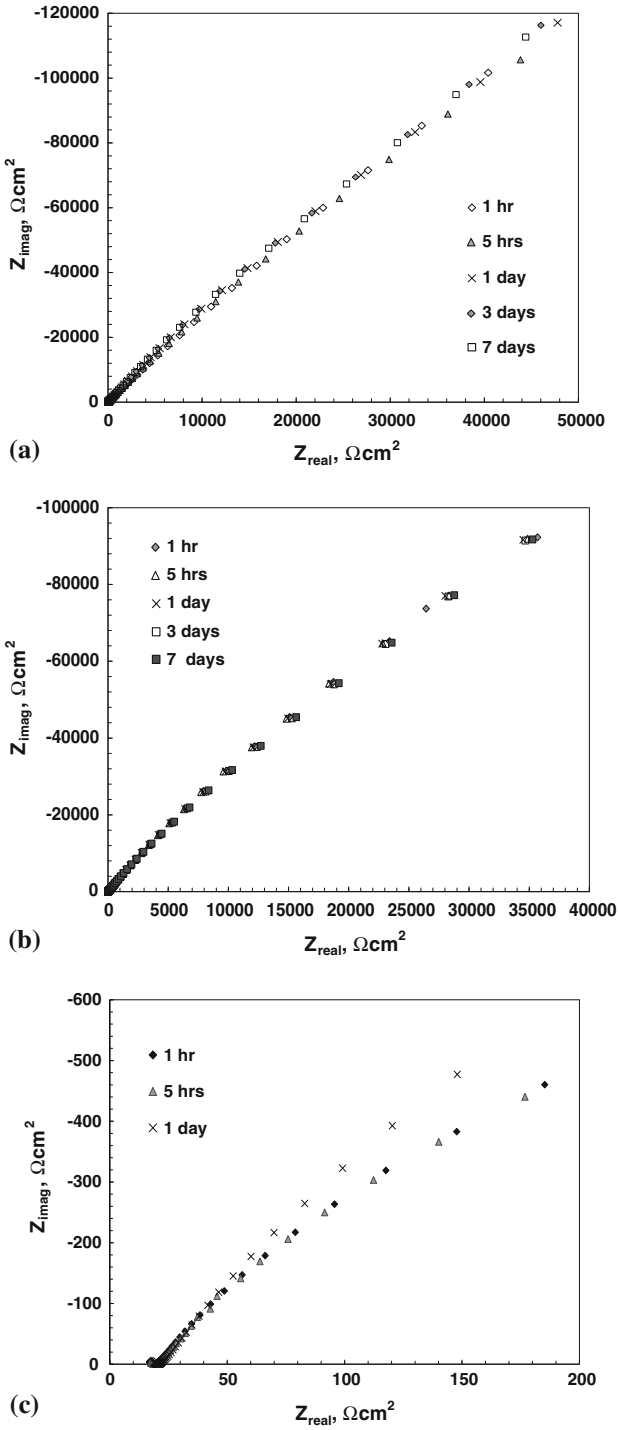

Fig. 5 Nyquist plots for the coating systems: CrN (a) CrSiCN-1 (b), and CrSiCN-2 (c)

acidity of the electrolyte in the pores tends to be higher than that in the bulk electrolyte due to the hydrolysis reaction (Ref 31), thus resulting in a higher concentration of chloride ion (Cl^-), and consequently a higher conductivity of the electrolyte in pores. Furthermore, the corrosion process in the pores is fast due to a large ratio of cathode to anode areas and the volume expansion associated with the formation of corrosion products induced enough stress causing fracture and further pit opening as seen in Fig. 7(b).

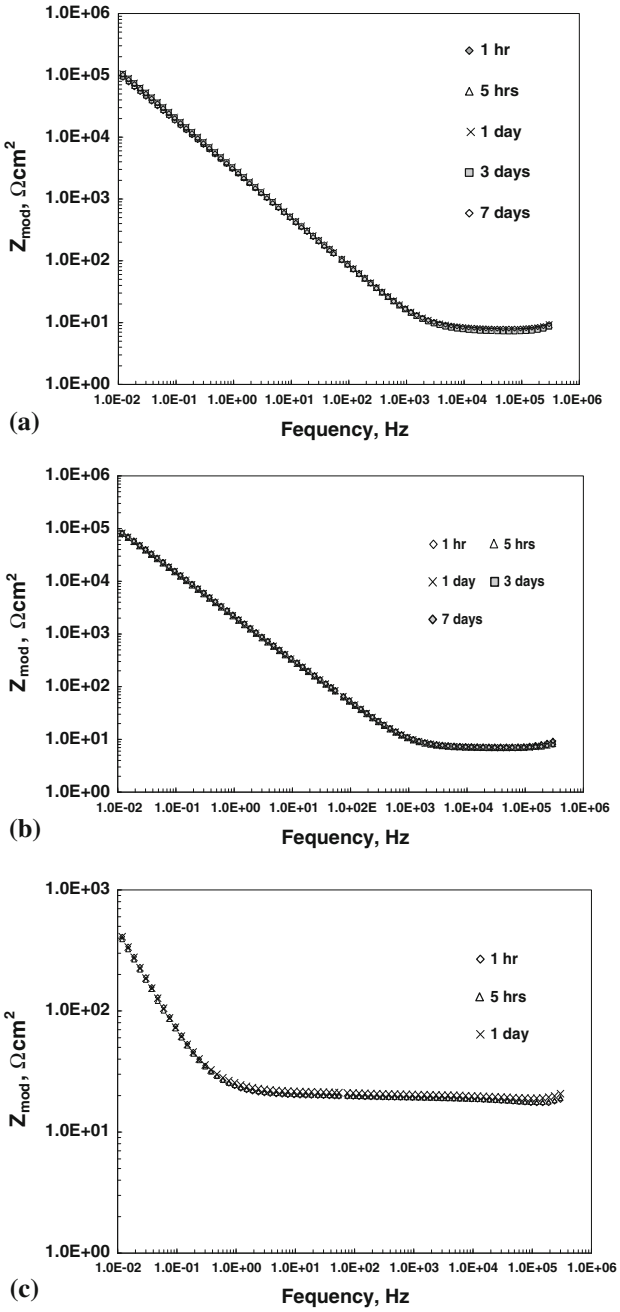

Fig. 6 Bode plots (log $|z|$ vs. log f) of the coatings: CrN (a), CrSiCN-1 (b), and CrSiCN-2 (c)

3.6 Equivalent electrical circuit analyses

EIS equivalent electrical circuit (EEC) approach was introduced to interpret the EIS spectra, and corrosion process took place in coatings containing defective sites. An equivalent circuit model was proposed as illustrated in Fig. 8, where R_e represents the resistance of electrolyte resistance, R_p is the resistance to current flow through the pores in the coating, and is inversely proportional to the porosity in the coating. In this EEC model, R_p is considered the most critical parameter in determining the corrosion resistance of the coatings, i.e., the resistance of penetration of electrolyte through the coating pores. A constant phase element (CPE) is incorporated in the EEC model to account for the nonideal electric behavior of the coating. Note that in a coating system, the CPE represents the capacitance of the coating. Its' admittance can be described in the form of Ref 32:

$$Y_0 - Q_c = C_c^0(1-P)A_c \quad \text{(Eq 3)}$$

where C_c^0 is normalized capacitance of coating, and remains unchanged during exposure; A_c is the exposed area of coating during testing; and P is the porosity of coating.

A co-tangent-hyperbolic diffusion impedance element (O) is involved to describe the diffusion impedance through the coating, and can be described as (Ref 32),

$$Y_0 - \mathrm{O}(\omega) = Y_0(j\omega)^{1/2} \cdot \cot anh[B(j\omega)^{1/2}] \quad \text{(Eq 4)}$$

where ω is angle frequency, B is the adjustable parameter of co-tangent-hyperbolic diffusion impedance element.

According to the EEC model, using Gamry Echem Analyst program (V. 1.35), the EIS data were fitted and the fitting results are displayed in Table 3.

With respect to the resistance R_p, it can be seen from Table 3 that in 3 days of immersion, the value for the coating CrN increased from 180 to 430 kΩ cm^2; and significantly, it increased from 670 to 1430 kΩ cm^2 for the coating CrSiCN-1. The coating CrSiCN-1 demonstrated a significant improvement in anticorrosion when compared to CrN. These behaviors stemmed from possible passivation stages occurred during immersion, and the formation of dense dielectric oxide on the coating surface may have limited mass transfer and ion current, thus increasing polarization resistance for the coating. These results are in agreement with those, e.g. passivation, in potentiodynamic polarization measurements. In contrast with those for coatings CrN and CrSiCN-1, the values of R_p for CrSiCN-2 remained to be low to 0.004 kΩ cm^2, indicating its poor anticorrosion performance because of the coating porosity and dual-phase structure. The exposure time did not have much impact on the coating performance in terms of R_p.

Admittance constant $(Y_0 - Q_c)$ is associated with the electrochemical properties of the coating surface features. According to Eq 4, values of admittance constant $(Y_0 - Q_c)$ have a proportional relationship with exposure area in coating. High values in admittance constant $(Y_0 - Q_c)$ indicate large areas of exposed coating due to the increased walls of pores. For the coatings CrN and CrSiCN-1, these values remained quite low (65 and 100 μF/cm^2, respectively) after 3 days of exposure; whereas the coating CrSiCN-2 exhibited much high values of over 3000 μF/cm^2. The low values of $(Y_0 - Q_c)$ for the coatings CrN and CrSiCN-1 stemmed from their relative small exposed areas in the coatings indicating dense microstructure. The much high values of $(Y_0 - Q_c)$ for the coating CrSiCN-2 is attributed to its relative large exposed area in the coating due to the porous structure, being in agreement with the early discussion on surface morphologies.

Empirical exponent $(n - Q_c)$ is determined by the interfacial characteristics of a surface or surface texture. The stable and similar values of $(n - Q_c)$ for the coatings CrN and CrSiCN-1 present their stable and similar solution-coating capacitive interface. Whereas, the lower values of $(n - Q_c)$ for the coating CrSiCN-2 indicate its "leaky capacitive" solution-coating interfacial characteristics (Ref 32), and this again is in agreement with its microstructure features.

With respect to the diffusion impedance $(Y_0 - \mathrm{O})$, the coating CrN remained low values of $(Y_0 - \mathrm{O})$ (about 130 μcm^2 Ω √s) and high values of B (about 1 √s). Whereas

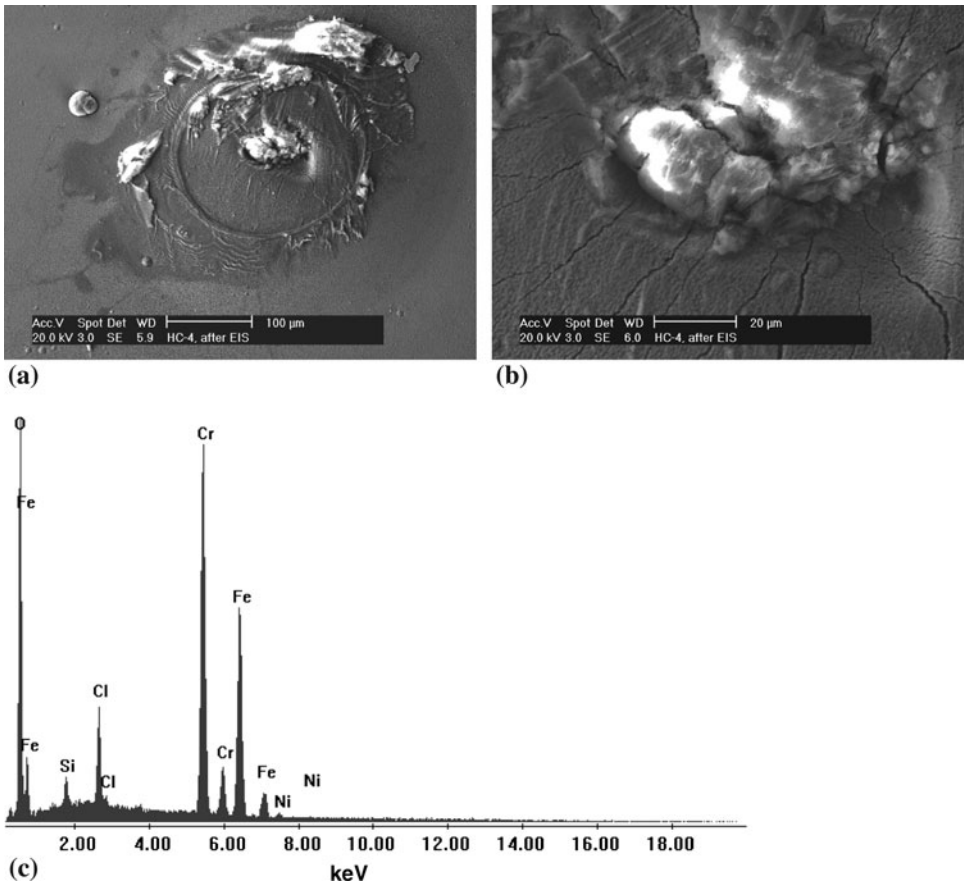

Fig. 7 Corrosion pits found on CrSiCN-2 surfaces after 24 h exposure (a) and (b), and EDS spectrum measured at the area covered by corrosion product (c)

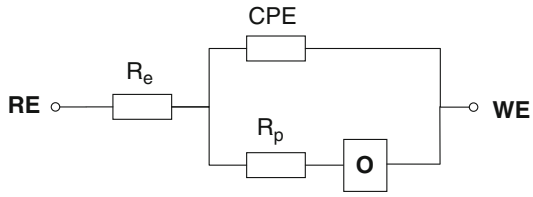

Fig. 8 Proposed equivalent circuit model for CrN-based series coatings corrosion

the values of $(Y_0 - O)$ for the coating CrSiCN-1 increased from 200 to 1100 μΩ cm^2 √s in 3 days of immersion, and the values of B remained to be low to 0.1 √s. These relationships are in agreement with that the increased values of $(Y_0 - O)$ are attributed to the decreased diffusion due to the corrosion product clogging pores in the coatings (Ref 32). For the coating CrSiCN-2, the relative high values of $(Y_0 - O)$ (over 500,000 μΩ cm^2 √s) and lower values of B (about 0.02 √s); and these could be associated with the coating structure-related resistance R_p that had very lower values. On one hand, the very

Table 3 Equivalent electrical circuit fitting data

Coating system	Exposed time	Re, Ω cm^2	$Y_0 - Q_c$, μF/cm^2	$n - Q_c$	R_p, kΩ cm^2	$Y_0 - O$, μ cm^{2}Ω√s	B, √s
CrN	1 h	9.28	58.5	0.862	181.9	218	0.4760
	3 h	9.07	63.3	0.853	386.6	122	0.9767
	5 h	8.93	65.3	0.852	400.7	123	1.1250
	1 day	9.00	67.3	0.856	369.8	126	0.9620
	3 days	9.22	70.1	0.850	429.4	137	0.9699
CrSiCN-1	1 h	7.06	98.3	0.833	667.0	218	0.1351
	5 h	6.99	100.3	0.830	929.4	844	0.0836
	1 day	6.87	101.2	0.827	1431.1	1,213	0.1343
	2 days	7.99	101.4	0.826	1424.0	1,178	0.1318
	3 days	6.81	100.5	0.827	1428.7	1,079	0.1248
CrSiCN-2	1 h	16.5	3141	0.424	4.3E−3	542,356	0.0238
	3 h	17.1	3597	0.450	4.0E−3	599,976	0.0219
	5 h	16.8	3361	0.423	4.6E−3	786,570	0.0172
	1 day	19.5	5633	0.610	3.6E−3	536,548	0.0211

low values of R_p would result in accelerated corrosion processes, thus large amount of corrosion product was generated at electrolyte-substrate interface. On the other hand, the corrosion product would clog the pores in the coating, thus causing increases in diffusion impedance (O), and consequently decreased the diffusion through the coating structure. However, in comparison with the resistance R_p, the diffusion impedance (O) is not dominant in the corrosion process at electrolyte-substrate interface, higher values of diffusion impedance (O) for the coating CrSiCN-2 did not benefit in anticorrosion performance when compared to the other two counterparts.

4. Conclusion

In this study, three CrN-based coatings were fabricated using magnetron sputtering technique. The microstructure and mechanical properties of the coatings were analyzed. All coatings were consisted of nanocrystalline grains with varying grain sizes depending on Si and C contents. The addition of 3.7 at.% Si in the coating resulted in the formation of crystalline Si_3N_4, unlike that reported in the literature. Electrochemical tests indicated that CrSiCN-1 had an improved anticorrosion performance when compared to CrN, while CrSiCN-2 demonstrated a poor corrosion resistance mainly due to its high coating porosity.

References

1. B. Navinšek and P. Panjan, Oxidation Resistance of PVD Cr, Cr-N and Cr-N-O Hard Coatings, *Surf. Coat. Technol.*, 1993, **59**, p 244–248
2. J. Stockeme, R. Winand, and P. Van den Brande, Comparison of Wear and Corrosion Behaviors of Cr and CrN Sputtered Coatings, *Surf. Coat. Technol.*, 1999, **115**, p 230–233
3. S.H. Yao and Y.L. Su, The Tribological Potential of CrN And Cr(C, N) Deposited by Multi-Arc PVD Process, *Wear*, 1997, **212**, p 85–94
4. Y. Chiba, T. Omura, and H. Ichimura, Wear Resistance of Arc Ion-Plated Chromium Nitride Coatings, *J. Mater. Res.*, 1993, **8**, p 1109–1115
5. B. Navinšek, P. Panjan, and I. Milošev, Industrial Applications of CrN (PVD) Coatings, Deposited at High and Low Temperatures, *Surf. Coat. Technol.*, 1997, **97**, p 182–191
6. P. Panjan, M. Čekada, R. Kirn, and M. Soković, Improvement of Die-Casting Tools with Duplex Treatment, *Surf. Coat. Technol.*, 2004, **180**, p 561–565
7. E. Lugscheider, O. Knotek, C. Barimani, S. Guerreiro, and H.K. Zimmermann, Cr-C-N Coatings Deposited with Different Reactive Carbon Carrier Gases in the Arc PVD Process, *Surf. Coat. Technol.*, 1997, **94–95**, p 416–421
8. G. Cholvy, J.L. Derep, and M. Gantois, Characterization and Wear Resistance of Coatings in the Cr-C-N Ternary System Deposited by Physical Vapour Deposition, *Thin Solid Films*, 1985, **126**, p 51–56
9. F. Schuster, F. Maury, J.F. Nowak, and C. Bernard, Carbonitride Coatings Deposited at Low Temperature by Organometallic Chemical Vapour Deposition, *Surf. Coat. Technol.*, 1991, **46**, p 275–288
10. Y.H. Yoo, J.H. Hong, J.G. Kim, H.Y. Lee, and J.G. Han, Effect of Si Addition to CrN Coatings on the Corrosion Resistance of CrN/Stainless Steel Coating/Substrate System in a Deaerated 3.5 Wt.% NaCl Solution, *Surf. Coat. Technol.*, 2007, **201**, p 9518–9523
11. D. Mercs, P. Briois, V. Demange, S. Lamy, and C. Coddet, Influence of the Addition of Silicon on the Structure and Properties of Chromium Nitride Coatings Deposited by Reactive Magnetron Sputtering Assisted by RF Plasmas, *Surf. Coat. Technol.*, 2007, **201**, p 6970–6976
12. E.Y. Choi, M.C. Kang, D.H. Kwon, D.W. Shin, and K.H. Kim, Comparative Studies on Microstructure and Mechanical Properties of CrN, Cr-C-N and Cr-Mo-N Coatings, *J. Mater. Process. Technol.*, 2007, **187–188**, p 566–570
13. G.A. Zhang, P.X. Yan, P. Wang, Y.M. Chen, and J.Y. Zhang, The Structure and Tribological Behaviors of CrN and Cr-Ti-N Coatings, *Appl. Surf. Sci.*, 2007, **253**, p 7353–7359
14. I.W. Park, D.S. Kang, J.J. Moore, S.C. Kwon, J.J. Rha, and K.H. Kim, Microstructures, Mechanical Properties, and Tribological Behaviors of Cr-Al-N, Cr-Si-N, and Cr-Al-Si-N Coatings by a Hybrid Coating System, *Surf. Coat. Technol.*, 2007, **201**, p 5223–5227
15. R. Wei, E. Langa, C. Rincon, and J.H. Arps, Deposition of Thick Nitrides and Carbonitrides for Sand Erosion Protection, *Surf. Coat. Technol.*, 2006, **201**, p 4453–4459
16. D.H. Boone, T.E. Strangman, and L.W. Wilson, Some Effects of Structure and Composition on the Properties of Electron Beam Vapor Deposited Coatings for Gas Turbine Superalloys, *J. Vac. Sci. Technol.*, 1974, **11**, p 641–646
17. I.I. Aksenov, V.M. Khoroshikh, N.S. Lomino, V.O. Ovcharenko, Yu.A. Zadneprovskij, Transformation of Axial Vacuum-Arc Plasma: Flows into Radial Streams and their Use in Coating Deposition Processes, *Proceedings of the 18th International Symposium on Discharges and Electrical Insulation in Vacuum*, 1998, Vol 2, p 566
18. J. Jeon, C. Jang, S. Yoon, B. Shin, and K. Kim, Effects of Si Addition on the Characteristic Evolution and Syntheses of Nanocomposite Cr-Si-C-N Coatings Prepared by a Hybrid Coating System, *Surf. Coat. Technol.*, 2005, **200**, p 1635–1639
19. S.-M. Yang, Y.-Y. Chang, D.-Y. Lin, D.-Y. Wang, and W. Wu, Mechanical and Tribological Properties of Multilayered TiSiN/CrN Coatings Synthesized by a Cathodic Arc Deposition Process, *Surf. Coat. Technol.*, 2008, **202**, p 2176–2181
20. H.O. Pierson, *Handbook of Refractory Carbides and Nitrides*, Noyes Publications, Westwood, NJ, 1996
21. L. Castaldi, D. Kurapov, A. Reiter, V. Shklover, P. Schwaller, and J. Patscheider, High Temperature Phase Changes and Oxidation Behavior of Cr-Si-N coatings, *Surf. Coat. Technol.*, 2007, **202**, p 781–785
22. J.W. Kim, K.H. Kim, D.B. Lee, and J.J. Moore, Study on High Temperature Oxidation Behaviors of Cr-Si-N Films, *Surf. Coat. Technol.*, 2006, **200**, p 6702–6705
23. J. Musil, P. Dohnal, and P. Zeman, Physical Properties and High Temperature Oxidation Resistance of Sputtered Si_3N_4/MoN_x Nanocomposite Coatings, *J. Vac. Sci. Technol. B*, 2005, **23**, p 1568–1575
24. C. Suryanarayana, M. Grant Norton, *X-Ray Diffraction A Practical Approach*, Plenum Press, New York, 1998
25. W.J. Chou, G.P. Yu, and J.H. Huang, Corrosion Resistance of ZrN Films on AISI, 304 Stainless Steel Substrate, *Surf. Coat. Technol.*, 2003, **167**, p 59–67
26. D.A. Jones, *Principles and Prevention of Corrosion*, Macmillan Publishing Company, New York, 1992
27. B. Matthes, E. Broszeit, J. Aromaa, H. Ronkainen, S.P. Hannula, A. Leyland, and A. Matthews, Corrosion Performance of Some Titanium-Based Hard Coatings, *Surf. Coat. Technol.*, 1991, **49**, p 489–495
28. F. Mansfeld, Electrochim. Acta, Electrochemical Impedance Spectroscopy (EIS) as a New Tool for Investigating, *Methods of Corrosion Protection*, 1990, **35**, p 1533–1544
29. C. Liu, Q. Bi, and A. Matthews, EIS Comparison on Corrosion Performance of PVD TiN and CrN Coated Mild Steel in 0.5 N NaCl Aqueous Solution, *Corros. Sci.*, 2001, **43**, p 195–1961
30. S.H. Ahn, Y.S. Choi, J.G. Kim, and J.G. Han, A Study on Corrosion Resistance Characteristics of PVD Cr-N Coated Steels by Electrochemical Method, *Surf. Coat. Technol.*, 2002, **150**, p 319–326
31. C.C. Lin, K.L. Chang, and H.C. Shih, Corrosive Behavior of Chromium Carbide-Based Films Formed on Steel Using a Filtered Cathodic Vacuum Arc System, *Appl. Surf. Sci.*, 2007, **253**, p 5011–5016
32. C. Liu, Q. Bi, A. Leyland, and A. Matthews, An Electrochemical Impedance Spectroscopy Study of the Corrosion Behaviour of PVD Coated Steels in 0.5 N NaCl Aqueous Solution: Part II.: EIS Interpretation of Corrosion Behaviour, *Corros. Sci.*, 2003, **45**, p 1257–1273